Fast Computation of Statistical Uncertainty for Spatiotemporal Distributions Estimated Directly from Dynamic Cone Beam SPECT Projections

Bryan W. Reutter[†], Grant T. Gullberg[‡], and Ronald H. Huesman[†]

[†]Center for Functional Imaging, Lawrence Berkeley National Laboratory
University of California, Berkeley, CA 94720, USA
[‡]Medical Imaging Research Laboratory, Department of Radiology
University of Utah, Salt Lake City, UT 84108, USA

I. Introduction

THE estimation of time-activity curves and kinetic model parameters directly from projection data is potentially useful for clinical dynamic single photon emission computed tomography (SPECT) studies, particularly in those clinics that have only single-detector systems and thus are not able to perform rapid tomographic acquisitions. Because the radiopharmaceutical distribution changes while the SPECT gantry rotates, projections at different angles come from different tracer distributions. A dynamic image sequence reconstructed from the inconsistent projections acquired by a slowly rotating gantry can contain artifacts that lead to biases in kinetic parameters estimated from time-activity curves generated by overlaying regions of interest on the images. If cone beam collimators are used and the focal point of the collimators always remains in a particular transaxial plane, additional artifacts can arise in other planes reconstructed using insufficient projection samples [1]. If the projection samples truncate the patient's body, this can result in additional image artifacts. To overcome these sources of bias in conventional image based dynamic data analysis, we and others have been investigating the estimation of time-activity curves and kinetic model parameters directly from dynamic SPECT projection data by modeling the spatial and temporal distribution of the radiopharmaceutical throughout the projected field of view [2–8].

In our previous work we developed a computationally efficient method for fully four-dimensional (4-D) direct estimation of spatiotemporal distributions from dynamic SPECT projection data [5], which extended Formiconi's least squares algorithm for reconstructing temporally static distributions [9]. In addition, we studied the biases that result from modeling various orders of temporal continuity and using various time samplings [5]. In the present work, we address computational issues associated with evaluating the statistical uncertainty of spatiotemporal model parameter estimates, and use Monte Carlo simulations to validate a fast algorithm for computing the covariance matrix for the parameters. Given this covariance matrix, the covariance between the time-activity curve models for the blood input function and tissue volumes of interest can be calculated and used to estimate compartmental model kinetic parameters more precisely, using nonlinear weighted least squares [10, 11].

This work was supported by the National Heart, Lung, and Blood Institute of the US Department of Health and Human Services under grants R01-HL50663 and P01-HL25840 and by the Director, Office of Science, Office of Biological and Environmental Research, Medical Sciences Division of the US Department of Energy under contract DE-AC03-76SF00098. This work was developed in part using the resources at the US Department of Energy National Energy Research Scientific Computing (NERSC) Center.

II. Fast Computation of Statistical Uncertainty for Spatiotemporal Distributions

Following our development in [5], time-varying activity concentrations within volumes of interest encompassing the projected SPECT field of view can be modeled by selecting a set of temporal basis functions capable of representing typical time variations and having desired smoothness properties. Similarly, the spatially nonuniform activity concentration within a particular volume of interest can be modeled by selecting an appropriate set of spatial basis functions. Given a set of temporal basis functions and sets of spatial basis functions for the volumes of interest, coefficients for the resulting spatiotemporal basis functions can be estimated directly from the SPECT projection data, along with the covariance matrix for the coefficients.

A. Covariance Matrix for the Spatiotemporal Basis Function Coefficients

Denoting the projection of the m^{th} spatial basis function along ray i at angle j by u_{ij}^m, and the integral of the n^{th} temporal basis function during the time interval associated with angle j of rotation k by v_{jk}^n, the projection equations can be expressed as

$$p_{ijk} = \sum_{m=1}^{M} \sum_{n=1}^{N} a_{mn} u_{ij}^m v_{jk}^n, \tag{1}$$

where the p_{ijk} are the modeled projections, the a_{mn} are the linear coefficients associated with the time integrals of the projections of the spatiotemporal basis functions, M is the number of spatial basis functions, and N is the number of temporal basis functions. The criterion which is minimized by varying the linear coefficients a_{mn} is the weighted sum of squares function

$$\chi^2 = \sum_{i=1}^{I} \sum_{j=1}^{J} \sum_{k=1}^{K} \frac{(p_{ijk}^* - p_{ijk})^2}{W_{ijk}}, \tag{2}$$

where the p_{ijk}^* are the measured projections, the W_{ijk} are weighting factors, I is the number of projection rays per angle,

J is the number of angles per rotation, and K is the number of rotations. Typically, the weighting factors are either unity for an unweighted fit or the estimated variances of the projections for a weighted fit.

Equations (1) and (2) can be rewritten in matrix form as

$$\mathbf{p} = \mathbf{F}\mathbf{a} \tag{3}$$

and

$$\chi^2 = (\mathbf{p}^* - \mathbf{F}\mathbf{a})^{\mathrm{T}}\mathbf{W}(\mathbf{p}^* - \mathbf{F}\mathbf{a}), \tag{4}$$

respectively, where $\mathbf{p}$ is an IJK element column vector whose $[i + (j-1)I + (k-1)IJ]^{\text{th}}$ element is p_{ijk}, $\mathbf{F}$ is an $IJK \times MN$ matrix whose $\{[i + (j-1)I + (k-1)IJ], [m + (n-1)M]\}^{\text{th}}$ element is $u_{ij}^m v_{jk}^n$, $\mathbf{a}$ is an MN element column vector whose $[m+(n-1)M]^{\text{th}}$ element is a_{mn}, $\mathbf{p}^*$ is an IJK element column vector whose $[i + (j-1)I + (k-1)IJ]^{\text{th}}$ element is p_{ijk}^*, and $\mathbf{W}$ is an $IJK \times IJK$ diagonal matrix whose $[i+(j-1)I + (k-1)IJ]^{\text{th}}$ diagonal element is $1/W_{ijk}$. The criterion, χ^2, is minimized by the vector of spatiotemporal basis function coefficients

$$\hat{\mathbf{a}} = (\mathbf{F}^{\mathrm{T}}\mathbf{W}\mathbf{F})^{-1}\mathbf{F}^{\mathrm{T}}\mathbf{W}\mathbf{p}^*. \tag{5}$$

The covariance matrix for the coefficients $\hat{\mathbf{a}}$ is

$$\mathrm{cov}(\hat{\mathbf{a}}) = (\mathbf{F}^{\mathrm{T}}\mathbf{W}\mathbf{F})^{-1}\mathbf{F}^{\mathrm{T}}\mathbf{W}\mathrm{cov}(\mathbf{p}^*)\mathbf{W}\mathbf{F}(\mathbf{F}^{\mathrm{T}}\mathbf{W}\mathbf{F})^{-1}, \tag{6}$$

where $\mathrm{cov}(\mathbf{p}^*)$ is the covariance matrix for the measured projections. Given an estimate of $\mathrm{cov}(\mathbf{p}^*)$, estimates of the statistical uncertainties of the coefficients $\hat{\mathbf{a}}$ are the square roots of the diagonal elements of the covariance matrix given by equation (6) and are denoted individually by $\hat{\sigma}_{\hat{a}_{mn}}$. In general, the errors in the coefficients are correlated and the covariance matrix given by equation (6) has nonzero elements off the diagonal.

For an unweighted least squares reconstruction of the spatiotemporal basis function coefficients $\hat{\mathbf{a}}$ (i.e., for $\mathbf{W}$ an identity matrix), an estimate of the symmetric $MN \times MN$ covariance matrix $\mathrm{cov}(\hat{\mathbf{a}})$ can be obtained quickly from equation (6) as follows. Assuming Poisson noise, the diagonal matrix having the modeled projections $\hat{\mathbf{p}} = \mathbf{F}\hat{\mathbf{a}}$ along the diagonal can be used as an estimate of the covariance matrix for the measured projections. Substituting this diagonal matrix for $\mathrm{cov}(\mathbf{p}^*)$ and the identity matrix for $\mathbf{W}$, equation (6) can be rewritten as

$$\mathrm{cov}(\hat{\mathbf{a}}) = (\mathbf{F}^{\mathrm{T}}\mathbf{F})^{-1}\mathbf{F}^{\mathrm{T}}\mathrm{diag}(\mathbf{F}\hat{\mathbf{a}})\mathbf{F}(\mathbf{F}^{\mathrm{T}}\mathbf{F})^{-1}. \tag{7}$$

We have presented a method for quickly calculating $(\mathbf{F}^{\mathrm{T}}\mathbf{F})^{-1}$ in [5]. Using a similar development, the symmetric $MN \times MN$ matrix $\mathbf{F}^{\mathrm{T}}\mathrm{diag}(\mathbf{F}\hat{\mathbf{a}})\mathbf{F}$ can be calculated quickly as follows. Denoting the $\{[m + (n-1)M], [m' + (n'-1)M]\}^{\text{th}}$ element of $\mathbf{F}^{\mathrm{T}}\mathrm{diag}(\mathbf{F}\hat{\mathbf{a}})\mathbf{F}$ by $\psi^{mnm'n'}$, one has

$$\psi^{mnm'n'} = \sum_{i=1}^{I}\sum_{j=1}^{J}\sum_{k=1}^{K} u_{ij}^m v_{jk}^n \times \left[\sum_{m''=1}^{M}\sum_{n''=1}^{N} \hat{a}_{m''n''} u_{ij}^{m''} v_{jk}^{n''}\right] \times u_{ij}^{m'} v_{jk}^{n'}, \tag{8}$$

where $\hat{a}_{m''n''}$ is the $[m'' + (n''-1)M]^{\text{th}}$ element of $\hat{\mathbf{a}}$, and "$\times$" denotes scalar multiplication. Rearranging the summations yields

$$\begin{aligned}\psi^{mnm'n'} &= \sum_{m''=1}^{M}\sum_{n''=1}^{N} \hat{a}_{m''n''} \times \sum_{j=1}^{J}\left[\sum_{i=1}^{I} u_{ij}^m u_{ij}^{m'} u_{ij}^{m''}\right]\left[\sum_{k=1}^{K} v_{jk}^n v_{jk}^{n'} v_{jk}^{n''}\right] \\ &= \sum_{m''=1}^{M}\sum_{n''=1}^{N} \hat{a}_{m''n''} \sum_{j=1}^{J} \alpha_j^{mm'm''}\beta_j^{nn'n''} \\ &= \sum_{m''=1}^{M}\sum_{n''=1}^{N} \hat{a}_{m''n''}\gamma^{mnm'n'm''n''},\end{aligned} \tag{9}$$

where the factors $\alpha_j^{mm'm''}$ and $\beta_j^{nn'n''}$ denote the summations $\sum_{i=1}^{I} u_{ij}^m u_{ij}^{m'} u_{ij}^{m''}$ and $\sum_{k=1}^{K} v_{jk}^n v_{jk}^{n'} v_{jk}^{n''}$, respectively, and the factor $\gamma^{mnm'n'm''n''}$ denotes the sum $\sum_{j=1}^{J} \alpha_j^{mm'm''}\beta_j^{nn'n''}$.

Using the factorization given by equation (9), it can be shown that most of the overhead associated with computing the symmetric matrix elements $\psi^{mnm'n'}$ lies in calculating the $\alpha_j^{mm'm''}$ factors and the $\gamma^{mnm'n'm''n''}$ factors. These calculations take about $[(I/N^3) + 1]JQ$ multiply-and-add operations, where $Q = (MN)^2(MN+1)/2$. By comparison, relatively straightforward computation of the summations given by equation (8) takes about $IJKQ$ multiply-and-add operations. Thus, for the computer simulations described in Section III, for which I/N^3 = 1/2, the factorization given by equation (9) reduces the computation by a factor of about $(2/3)IK \approx 20{,}000$.

B. Covariance Between Integrated Time-Activity Curve Model Segments

Given an estimate of $\mathrm{cov}(\hat{\mathbf{a}})$, the covariance matrix for the spatiotemporal basis function coefficients, estimates of the covariance between integrated segments of the time-activity curve models for the volumes of interest can be obtained as follows.

The integral of the time-activity curve model for volume of interest m, during the time interval associated with angle j of rotation k, can be expressed as $\sum_{n=1}^{N} \hat{a}_{mn} v_{jk}^n$. Thus, the covariance of this time integral with the time integral associated with volume of interest m' during angle j' of rotation k' is

$$\begin{aligned}&\mathrm{cov}\left(\sum_{n=1}^{N} \hat{a}_{mn} v_{jk}^n, \sum_{n=1}^{N} \hat{a}_{m'n} v_{j'k'}^n\right) \\ &\qquad = \sum_{n=1}^{N}\sum_{n'=1}^{N} v_{jk}^n \,\mathrm{cov}(\hat{a}_{mn}, \hat{a}_{m'n'})\, v_{j'k'}^{n'},\end{aligned} \tag{10}$$

and the variance of each time integral is

$$\begin{aligned}\sigma_{jkm}^2 &= \mathrm{var}\left(\sum_{n=1}^{N} \hat{a}_{mn} v_{jk}^n\right) \\ &= \sum_{n=1}^{N}\sum_{n'=1}^{N} v_{jk}^n \,\mathrm{cov}(\hat{a}_{mn}, \hat{a}_{mn'})\, v_{jk}^{n'}.\end{aligned} \tag{11}$$

As a figure of merit related to the global precision of the time-activity curve model for volume of interest m, the following expression yields a squared noise-to-signal ratio calculated as the mean (over all of the time segments) of the expected values of the squared errors between the integrated segments of the "true" and modeled curves, normalized by the mean square value of the integrated segments of the "true" curve:

$$\xi_m^2 = \frac{\sum_{j=1}^{J}\sum_{k=1}^{K}\sigma_{jkm}^2}{\sum_{j=1}^{J}\sum_{k=1}^{K}\left[\sum_{n=1}^{N}\hat{a}_{mn}v_{jk}^n\right]^2}. \qquad (12)$$

Substituting equation (11) into equation (12), the squared noise-to-signal ratio ξ_m^2 can be calculated quickly by rearranging the summations, precomputing the inner products of the temporal basis functions, $\nu^{nn'} = \sum_{j=1}^{J}\sum_{k=1}^{K} v_{jk}^n v_{jk}^{n'}$, and exploiting the symmetry with respect to the indices n and n':

$$\xi_m^2 = \frac{\sum_{n=1}^{N}\sum_{n'=1}^{N}\mathrm{cov}(\hat{a}_{mn},\hat{a}_{mn'})\nu^{nn'}}{\sum_{n=1}^{N}\sum_{n'=1}^{N}\hat{a}_{mn}\hat{a}_{mn'}\nu^{nn'}}. \qquad (13)$$

III. Computer Simulations

To validate the fast algorithm presented in Section II, 1600 realizations of cone beam projection data having Poisson noise were generated using the simulation apparatus described in [5].

Simulated spatiotemporal distributions were obtained using the Mathematical Cardiac Torso (MCAT) phantom developed at the University of North Carolina [12]. The emission phantom (Fig. 1) was composed of 128 contiguous 1.75 mm-thick slices and contained the blood pool, three myocardial tissue volumes of interest (normal myocardium, septal defect, and lateral defect), liver, and background tissue. Projections were attenuated using the corresponding MCAT attenuation phantom.

The simulated time-activity curves (Fig. 2) mimicked the kinetics of teboroxime [13]. The simulated 15 min data acquisition consisted of $I = 2048$ cone beam projection rays per angle (64 transverse $\times$ 32 axial), $J = 120$ angles per revolution, and $K = 15$ revolutions, and thus yielded about 3.7 million projection samples. The projection bins were 7 mm $\times$ 7 mm at the detector, and the detector was 30 cm from the center of the field of view. The cone beam collimators had a hole diameter of 2 mm, a length of 4 cm, and were offset 1 cm from the detector. The focal length was 70 cm, which resulted in truncation of the data (Fig. 1). Attenuation and geometric point response were modeled using a ray-driven projector with line length weighting [14]. Scatter was not modeled. The amplitude of the simulated blood input function was adjusted so that about 10 million events were detected using the cone beam collimators.

The spatial basis projection factors u_{ij}^m were defined by forward projecting each of the six known emission volumes composing the MCAT phantom (Fig. 1). Each emission volume was modeled to contain spatially uniform activity, which yielded $M = 6$ sets of spatial basis projection factors.

The temporal basis integral factors v_{jk}^n were defined by integrating $N = 16$ splines spanning 15 time segments having geometrically increasing length (Fig. 3). Piecewise quadratic B-splines were used with an initial time segment length of 10 sec. The resulting curve models were continuous through their first derivative and yielded errors of less than 2% for noiseless projections, where the error was defined to be the root mean square (rms) difference between the simulated curve and the spline model, normalized by the rms value of the simulated curve [5].

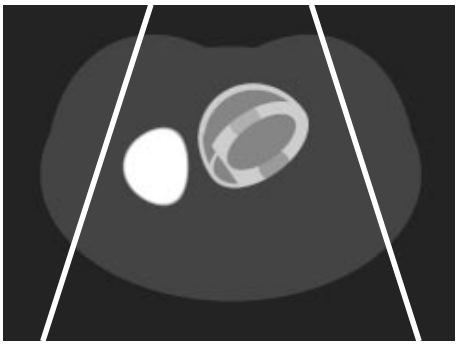

Fig. 1. Transverse cross section through the MCAT emission phantom, showing the truncation of data resulting from the use of cone beam collimators.

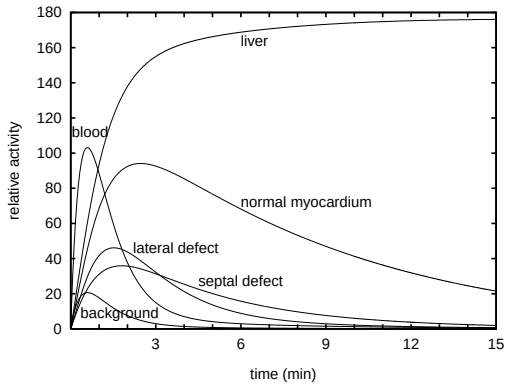

Fig. 2. Simulated time-activity curves for the volumes shown in Fig. 1.

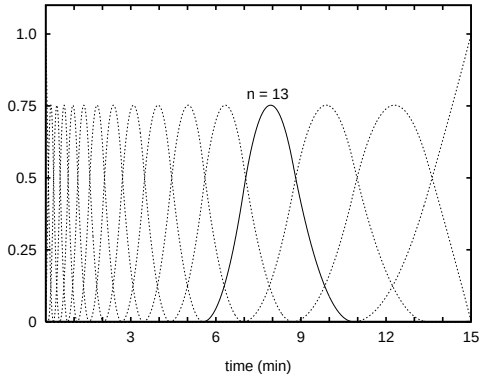

Fig. 3. Piecewise quadratic B-spline temporal basis functions. Sixteen splines are used to span 15 time segments having geometrically increasing length. The initial time segment length is 10 sec. The thirteenth spline is shown as a solid curve.

The computational benefit of using the factorization given by equation (9) to estimate the covariance matrix for the spatiotemporal basis function coefficients was evident in the simulations. The number of multiply-and-add operations used to calculate $\mathbf{F}^{\mathrm{T}}\mathrm{diag}(\mathbf{F}\hat{\mathbf{a}})\mathbf{F}$ was reduced from about 1.6 trillion to about 80 million. Using a 194-MHz R10000-based SGI workstation, it took 34 sec to estimate the 96 coefficients for the spatiotemporal basis functions, their covariance matrix, and the squared noise-to-signal ratios given by equation (13).

TABLE I

ACTUAL AND ESTIMATED STATISTICAL UNCERTAINTIES FOR SPATIOTEMPORAL BASIS FUNCTION COEFFICIENTS, FOR 1600 REALIZATIONS OF NOISY PROJECTIONS. THE SAMPLE STANDARD DEVIATIONS OF THE COEFFICIENTS (THE SECOND COLUMN IN EACH OF THE FOUR SUB-TABLES) AGREE CLOSELY WITH THE SAMPLE MEANS OF THE ESTIMATED STATISTICAL UNCERTAINTIES (THE THIRD COLUMN IN EACH OF THE FOUR SUB-TABLES).

n	blood pool			normal myocardium			septal defect			lateral defect		
	$\hat{a}_{1n}$		$\hat{\sigma}_{\hat{a}_{1n}}$	$\hat{a}_{2n}$		$\hat{\sigma}_{\hat{a}_{2n}}$	$\hat{a}_{3n}$		$\hat{\sigma}_{\hat{a}_{3n}}$	$\hat{a}_{4n}$		$\hat{\sigma}_{\hat{a}_{4n}}$
	sample mean	sample sdev	sample mean	sample mean	sample sdev	sample mean	sample mean	sample sdev	sample mean	sample mean	sample sdev	sample mean
1	0.279	0.128	0.131	0.0102	0.166	0.166	-0.0529	1.28	1.29	-0.212	0.747	0.762
2	5.20	0.138	0.140	1.05	0.171	0.174	0.559	1.33	1.35	0.979	1.47	1.46
3	7.65	0.157	0.160	2.30	0.185	0.187	1.36	1.89	1.88	1.38	3.00	2.99
4	8.20	0.172	0.175	3.75	0.331	0.333	1.89	3.04	3.05	2.42	1.95	1.95
5	7.19	0.153	0.160	5.15	0.222	0.219	2.33	1.91	1.94	3.25	1.26	1.27
6	5.40	0.105	0.107	6.30	0.148	0.145	2.70	1.20	1.24	3.58	1.75	1.73
7	3.51	0.0974	0.0953	7.07	0.141	0.140	2.87	1.50	1.54	3.59	0.876	0.864
8	2.00	0.0658	0.0668	7.36	0.108	0.109	2.67	0.886	0.904	3.11	1.08	1.09
9	1.04	0.0545	0.0543	7.21	0.0839	0.0836	2.45	0.600	0.602	2.44	0.593	0.602
10	0.535	0.0464	0.0446	6.71	0.0743	0.0735	2.02	0.560	0.562	1.69	0.418	0.411
11	0.308	0.0361	0.0362	5.98	0.0632	0.0628	1.57	0.486	0.477	1.03	0.364	0.354
12	0.208	0.0305	0.0298	5.13	0.0538	0.0530	1.13	0.397	0.399	0.592	0.296	0.300
13	0.149	0.0250	0.0245	4.20	0.0454	0.0441	0.761	0.327	0.325	0.307	0.258	0.253
14	0.103	0.0197	0.0201	3.28	0.0360	0.0365	0.478	0.268	0.270	0.179	0.206	0.207
15	0.0657	0.0167	0.0168	2.39	0.0303	0.0308	0.268	0.232	0.234	0.0853	0.165	0.170
16	0.0399	0.0169	0.0169	1.64	0.0314	0.0313	0.135	0.270	0.269	0.0651	0.161	0.164

TABLE II

ACTUAL AND ESTIMATED NOISE-TO-SIGNAL RATIOS FOR TIME-ACTIVITY CURVES, FOR 1600 REALIZATIONS OF NOISY PROJECTIONS.

	noise-to-signal ratio (%)		ξ_m (%)	
	sample mean	sample sdev	sample mean	sample sdev
blood pool	1.51	0.35	1.56	0.008
normal myocardium	1.13	0.27	1.16	0.003
septal defect	32.5	9.1	32.5	2.6
lateral defect	28.5	8.0	28.6	2.3
liver	0.167	0.031	0.170	0.0001
background	0.242	0.058	0.247	0.0002

Table I shows that the sample means of the $\hat{\sigma}_{\hat{a}_{mn}}$ (the square roots of the diagonal elements of the estimated covariance matrix) were within 5% of the sample standard deviations of the $\hat{a}_{mn}$ (the estimated spatiotemporal basis functions coefficients), for the blood pool and myocardial tissue volumes. For the liver and background tissue, the agreement was to within 4%. The coefficients of variation for the $\hat{\sigma}_{\hat{a}_{mn}}$ were less than 2%.

Table II shows that the sample means of the ξ_m (the estimated noise-to-signal ratios) were within 4% of the sample means of the rms differences between the 1600 sets of time-activity curve models and their corresponding mean curves, normalized by the rms values of the mean curves. The time-activity curves for the septal and lateral defects exhibited the largest variability, because of their small spatiotemporal support.

IV. FUTURE DIRECTIONS

The fast algorithm presented in Section II will facilitate the study of the statistical variability that results from modeling various orders of temporal continuity and using various time samplings, when estimating time-activity curves directly from dynamic cone beam SPECT projections. It may also allow compartmental model kinetic parameters to be estimated from the curves more precisely, using nonlinear weighted least squares.

ACKNOWLEDGMENT

The authors thank the University of North Carolina Medical Imaging Research Laboratory for making the MCAT phantom available.

This work was supported by the National Heart, Lung, and Blood Institute of the US Department of Health and Human Services under grants R01-HL50663 and P01-HL25840 and by the Director, Office of Science, Office of Biological and Environmental Research, Medical Sciences Division of the US Department of Energy under contract DE-AC03-76SF00098. This work was developed in part using the resources at the US Department of Energy National Energy Research Scientific Computing (NERSC) Center.

REFERENCES

[1] H K Tuy, "An inversion formula for cone-beam reconstruction," *SIAM J Appl Math*, vol. 43, no. 3, pp. 546–552, 1983.

[2] R H Huesman, B W Reutter, G L Zeng, and G T Gullberg, "Kinetic parameter estimation from SPECT cone-beam projection measurements," *Phys Med Biol*, vol. 43, no. 4, pp. 973–982, 1998.

[3] G T Gullberg, R H Huesman, S G Ross, E V R Di Bella, G L Zeng, B W Reutter, P E Christian, and S A Foresti, "Dynamic cardiac single-photon emission computed tomography," in *Nuclear Cardiology: State of the Art and Future Directions*, B L Zaret and G A Beller, Eds., chapter 11, pp. 137–187. Mosby Inc, St Louis, 1999.

[4] A Sitek, E V R Di Bella, and G T Gullberg, "Reconstruction from slow rotation dynamic SPECT using a factor model," in *Information Processing in Medical Imaging: Proceedings of the Sixteenth International Conference*, A Kuba, M Šámal, and A Todd-Pokropek, Eds., 1999, pp. 436–441.

[5] B W Reutter, G T Gullberg, and R H Huesman, "Direct least-squares estimation of spatiotemporal distributions from dynamic SPECT projections using a spatial segmentation and temporal B-splines," *IEEE Trans Med Imag*, vol. 19, no. 5, pp. 434–450, 2000.

[6] J S Maltz, "Direct recovery of regional tracer kinetics from temporally inconsistent dynamic ECT projections using dimension-reduced time-activity basis," *Phys Med Biol*, vol. 45, no. 11, pp. 3413–3429, 2000.

[7] A Celler, T Farncombe, C Bever, D Noll, J Maeght, R Harrop, and D Lyster, "Performance of the dynamic single photon emission computed tomography (dSPECT) method for decreasing or increasing activity changes," *Phys Med Biol*, vol. 45, no. 12, pp. 3525–3543, 2000.

[8] T Farncombe, A Celler, C Bever, D Noll, J Maeght, and R Harrop, "The incorporation of organ uptake into dynamic spect (dSPECT) image reconstruction," *IEEE Trans Nucl Sci*, vol. 48, no. 1, pp. 3–9, 2001.

[9] A R Formiconi, "Least squares algorithm for region-of-interest evaluation in emission tomography," *IEEE Trans Med Imag*, vol. 12, no. 1, pp. 90–100, 1993.
[10] R H Huesman and B M Mazoyer, "Kinetic data analysis with a noisy input function," *Phys Med Biol*, vol. 32, no. 12, pp. 1569–1579, 1987.
[11] D J Kadrmas, E V R Di Bella, R H Huesman, and G T Gullberg, "Analytical propagation of errors in dynamic SPECT: Estimators, degrading factors, bias and noise," *Phys Med Biol*, vol. 44, no. 8, pp. 1997–2014, 1999.
[12] B M W Tsui, J A Terry, and G T Gullberg, "Evaluation of cardiac cone-beam single photon emission computed tomography using observer performance experiments and receiver operating characteristic analysis," *Invest Radiol*, vol. 28, no. 12, pp. 1101–1112, 1993.
[13] R K Narra, T Feld, and A D Nunn, "Absorbed radiation dose to humans from technetium-99m-teboroxime," *J Nucl Med*, vol. 33, no. 1, pp. 88–93, 1992.
[14] G L Zeng, G T Gullberg, B M W Tsui, and J A Terry, "Three-dimensional iterative reconstruction algorithms with attenuation and geometric point response correction," *IEEE Trans Nucl Sci*, vol. 38, no. 2, pp. 693–702, 1991.

DISCLAIMER